Dynamic Real-Time Optimization with Product Quality Considerations and Closed-loop Prediction: Application to the Tennessee Eastman Benchmark

Ali M. Sahlodin[a,*], Ramin Bozorgmehry Boozarjomehry[b], Mohammad Fakhroleslam[c]

[a] *Process Systems Engineering Laboratory, Department of Chemical Engineering, Amirkabir University of Technology (Tehran Polytechnic), PO Box 1591634311, Tehran, Iran*
[b] *Department of Chemical and Petroleum Engineering, Sharif University of Technology, PO Box 11365-8639, Tehran, Iran*
[c] *Process Engineering Department, Faculty of Chemical Engineering, Tarbiat Modares University, PO Box 14115-111, Tehran, Iran*

Abstract

Conventional real-time optimization (RTO) algorithms provide steady-state set points at which the process would operate economically. However, the process may undergo severe economic losses (e.g., off-specification production) when transitioning from the nominal steady state to the optimal one. In this paper, a dynamic RTO (DRTO) strategy accounting for the total cost of set point transitions is developed for the Tennessee Eastman process. The objective function of the DRTO is defined as the integral of the sum of operating costs and the costs of producing off-specification products. A closed-loop prediction model is employed to estimate future process outputs required to evaluate the DRTO objective function and constraints. The results reaffirm that the off-specification cost should not be ignored in the optimization as it constitutes up to 80% of the total cost. Moreover, the proposed DRTO is shown to strike a reasonable balance between the operating and the off-specification costs, yielding significant economic saving (up to 28%) over conventional RTO that considers the steady-state operating cost only. The saving is more pronounced when the process faces sustained disturbances. Interestingly, the DRTO finally reaches the same steady-state operating cost as the conventional RTO, ensuring no extra costs imposed on the long-term plant operation.

***Keywords**:* Online optimization; Economic optimization; Product quality; Process transition; Tennessee Eastman; Economic Model predictive control.

---

[*] Corresponding author. Email: sahlodin@aut.ac.ir , Tel: +98 21 6454 3154.

1. Introduction

The volatile market, tough competition, and high cost of energy are factors that have pushed production companies to reduce costs using data, models, and digitalization [1]. To this end, process optimization, such as real-time optimization (RTO), has gained increasing attention over the past few decades [2–4]. Generally, any control system designed for economic optimization of processes is referred to as RTO [5]. RTO algorithms continuously estimate operating conditions based on a process model and compute economically optimal set points. A standard RTO system involves a steady-state model, a set of process constraints, an adaptation law for the process model, and an economic optimization problem [6].

To date, many researchers have focused on RTO and its application to various systems (refer to [7,8] for some recent examples). RTO has been examined from a variety of perspectives including modeling methods such as data-driven modeling [9,10], data reconciliation [11], RTO structure [12], and dynamic RTO (DRTO) [13,14]. DRTO is an extension of the conventional RTO that incorporates process dynamics into the optimization through prediction of the process future behavior. It allows for optimizing the process (transient) economics over the entire operation span, unlike the conventional RTO that considers steady-state economics only, potentially leading to costly transitions. Therefore, DRTO can improve operational efficiency by adapting to time-varying conditions [15]. This makes it a promising technique in the online optimization of processes subject to time-varying operating conditions.

DRTO can act as a supervisory layer over the regulatory control system. In some publications, DRTO is used in conjunction with model predictive control (MPC) as the regulatory layer. In particular, Jamaludin and Swartz [16,17] proposed a closed-loop DRTO (CL-DRTO) scheme with MPC embedded as the regulatory control system, resulting in a bilevel dynamic optimization problem. To reduce the computational complexity, they reformulated the problem into single-level optimization by replacing the embedded MPC problem with its Karush-Kuhn-Tucker (KKT) necessary optimality conditions. In these studies, a small-scale polymer grade transition reactor served as a case study, demonstrating the DRTO's objective of maximizing the target grade on-specification production and minimizing control system input costs. The necessary condition of optimality was also used in [18] to improve the DRTO results in the face of plant model uncertainties.

Ramesh et al. [19] applied a CL-DRTO with a stabilizing MPC in the regulatory layer. The DRTO layer was kept separate from the regulatory layer to enable the use of the existing hierarchical control architecture. The MPC layer was posed as an inner optimization within the DRTO, resulting in a bi-level optimization, which is very expensive computationally. They used a linear prediction model in the MPC layer, which can result in considerable model mismatch in nonlinear systems. Also, due to the multi-layer architecture, the CL-DRTO would exhibit computational challenges if applied to large-scale processes. Kim and Lima [20] applied DRTO to a relatively large-scale energy production plant aiming at optimizing environmental and operating costs. Nonetheless, their prediction model for the DRTO was a simplified data-driven regression model, rather than a nonlinear first-principles model. Data-driven models are known to have limitations outside the range of training data.

The practicality of DRTO has been underscored by case studies in various industries ranging from chemical processing [13,21] to energy systems [22,23]. The increasing availability of high-performance computers has facilitated the viability of DRTO, encouraging further research on DRTO algorithms and applications. MacKinnon et al. [24] addressed CL-DRTO for open-loop unstable systems by utilizing a stabilizing

MPC in the regulatory layer. Pataro et al. [25] presented CL-DRTO with an underlying advanced control layer for a bioethanol distillation column.

Despite the above-mentioned advancements, the application of DRTO has been mostly limited to single-equipment units or small-scale processes. With small-scale applications, however, many of the challenges of implementing DRTO would not be encountered. For example, high process dynamic interactions, open-loop instability, and lack of a rigorous closed-loop prediction model are the challenges associated with large-scale processes and should be addressed in DRTO applications of a realistic size. The Tennessee Eastman (TE) process [26] is a relatively large-scale benchmark compared with the case studies presented in the literature. While applications of conventional RTO to the TE process can be found in the literature, to the authors' best knowledge, no application of DRTO to the TE process has been reported in the literature. An online dynamic optimization scheme for the TE process was presented in [27] for the purpose of examining the performance of large-scale nonlinear programming solvers. Although the work could resemble DRTO from a mathematical standpoint, it would not be classified as such because the problem was formulated as a tracking MPC problem instead of an economic optimization problem, which is a distinctive point in (D)RTO formulations. Conventional RTO developed for the TE process can be found in, e.g., [28–32], where steady-state operating cost was used in the online optimization. However, the transient costs, including operations and off-specification costs, can significantly overshadow steady-state costs, a consideration that is addressed in the proposed DRTO by combining both costs into the objective function.

In this study, a DRTO strategy for the TE process is developed. The off-specification cost and the overall plant operating cost are considered as the objective functions. The regulatory control layer consists of proportional-integral (PI) controllers. The proposed

DRTO utilizes closed-loop prediction, which is built upon a reduced-order nonlinear dynamic model of the process augmented with PI controllers. The PI controllers impose no extra computational cost, yielding an efficient closed-loop prediction. It is shown that the proposed DRTO effectively reduces the total grade transition cost despite process disturbances and clearly outperforms conventional RTO presented for the same process.

2. Tennessee Eastman Process

This section presents an overview of the TE process along with its control structure and reduced-order nonlinear model.

2.1. Process description

The TE process [26] has been used as a complex benchmark for control, optimization, fault detection, and machine learning applications (see e.g., [33–35]). It consists of five major unit operations: a two-phase reactor, a product condenser, a recycle compressor, a separator, and a stripper. This process along with its control system is depicted in Figure 1.

Figure 1. The Tennessee Eastman process and its control system [26,36]; figure taken and adapted from the open-access article [37].

The reactor hosts four exothermic irreversible reactions as

$$A(g)+C(g)+D(g) \longrightarrow G(liq) \qquad \text{Product 1}$$

$$A(g)+C(g)+E(g) \longrightarrow H(liq) \qquad \text{Product 2}$$

$$A(g)+E(g) \longrightarrow F(liq) \qquad \text{Byproduct}$$

$$3D(g) \longrightarrow 2F(liq) \qquad \text{Byproduct,}$$

where G and H denote the desired products, B is an inert component, and F is a byproduct. Together with the reactants (A, C, D, and E), the process contains a total of eight components, of which A, B, and C are effectively non-condensable and always in the vapor phase. After partial condensation in the condenser, the reactor effluent is separated to liquid and gas streams in the separator. To prevent the buildup of unwanted components, including the inert, the gas stream is partially purged, then compressed and recycled to the reactor. The separator liquid stream is sent to the stripper to separate and recycle the reactants D and E back to the reactor. The stripper bottom stream contains mainly the products G and H.

The process, as originally coded in FORTRAN by [26], has 12 inputs (manipulated variables) and 41 outputs (measurements), all corrupted by zero-mean white noise. The stream compositions are output for Streams 6, 9, and 11 only, and the other stream compositions are made unknown to the user. Details of the process outputs and inputs can be found in [26,28].

McAvoy and Ye [36] proposed a control system for the TE process consisting of PI controllers mostly configured as cascade loops. The loop configurations are illustrated in Figure 1, with details such as controller tunings found in [28,36].

2.2. Nonlinear dynamic model

The actual model equations for the TE process have not been published by its inventors. Ricker and Lee [38] developed a reduced-order first-principles nonlinear dynamic model for the TE process that included only material balances. The need for energy balance is removed by adding fast temperature controllers. Consequently, the separator and reactor temperatures are turned from output to input variables. The reduced-order model by [38] can be written in the form of differential-algebraic equations (DAEs) as

$$\dot{\boldsymbol{x}} = \boldsymbol{f}(\boldsymbol{x}, \boldsymbol{u}, \boldsymbol{d}), \quad (1)$$
$$\boldsymbol{y} = \boldsymbol{g}(\boldsymbol{x}, \boldsymbol{u}, \boldsymbol{d}),$$

where $\boldsymbol{x^T} = [N_{A,r}, N_{B,r}, \dots, N_{H,r}, N_{A,s}, N_{B,s}, \dots, N_{H,s}, N_{A,m}, N_{B,m}, \dots, N_{H,m}, N_{G,p}, N_{H,p}]^T$ consists of 26 state variables (molar holdup in kmol), with the first subscript *A*, *B*,…, and *H* denoting the component name, and the second subscript *r*, *s*, *m*, and *p* denoting the reactor, separator, feed mixing zone, and product reservoir, respectively; $\boldsymbol{u^T} = [F_1, F_2, F_3, F_4, F_8, F_9, F_{10}^p, F_{11}, T_{cr}, T_{cs}]^T$ is the vector of 10 manipulated variables, with F_i designating the molar flow rate of Stream i in kmol/h, and T_{cr} and T_{cs} being the reactor and separator temperatures in °C; $\boldsymbol{d}$ consists of 15 unmeasured (possibly time-varying) process parameters; $\boldsymbol{y}$ is composed of 23 process output variables. The list of the model inputs, outputs, and parameters along with the full model equations is found in [28,38].

The online estimation of the model's state variables and parameters is carried out using a constant-gain extended Kalman filter (EKF), details of which are presented in [28,38] and not repeated here for space limitations. The estimated states and parameters are utilized to initialize the prediction model when the real-time optimizer is triggered.

3. Proposed Dynamic Real-time Optimization

The DRTO algorithm for the TE process is discussed in this section. The transient product quality is accounted for by including the loss of off-specification products in the economic objective function. The objective function is formulated as the integral of the predicted operating and off-specification costs up to the prediction horizon. The proposed DRTO features a closed-loop prediction model with PI loops for predicting the process future behavior. The entire DRTO system is illustrated in Figure 2. The plant measurements are sent to the EKF in order to update estimates of the model states and parameters. The estimated values from the EKF along with the set points guessed by the optimizer are used to initialize and run the prediction model over the prediction horizon. The model predictions are then sent to the optimizer for the evaluation of the objective function and constraints. The iterations between the optimizer and the prediction model continue until the optimizer converges. Then, the optimal set points are sent to the control system after being passed through first-order filters with a time constant of 7.0 h. The filters are meant to smooth out sudden operational moves and prevent possible instability [28]. In case the optimization fails to converge to optimal set points at the current execution time, the optimal set points obtained from the previous execution time are sent to the plant. Details of the objective function, decision variables, and problem constraints are presented in the following subsections. The resulting dynamic optimization problem is solved using the sequential approach [39].

Figure 2. Proposed DRTO procedure.

3.1. Objective function

Golshan et al. [28–30] used the steady-state operating cost as the objective function. In this work, however, the objective function is different in two ways. First, a cumulative, instead of an instantaneous, cost is considered, and second, the off-specification cost is also included. Problem (2) defines the DRTO formulation, where the objective is to minimize the cumulative sum of operating and off-specification costs over a finite prediction horizon:

$$\underset{X \in [X^L, X^U]}{\text{Minimize}} \; f(X) = \int_{t_1}^{t_2} (OC + OSC)dt, \tag{2}$$

Subject to:

Dynamic prediction model

Path constraints

where X is the vector of decision variables (see Subsection 3.2); OC and OSC denote the instantaneous operating cost and off-specification cost, respectively; t_1 is the current time, at which the optimizer is set to be executed; t_2 is the time up to which the sum of the two costs is integrated, i.e., t_2- t_1 is the prediction horizon. The instantaneous operating cost (OC) sums the cost of all the components (except inert) wasted from the purge stream, the cost of some of the non-product components wasted from the product stream, and the cost of utilities defined as [26]

$$OC(\$\,\mathrm{h}^{-1}) = F_9 \sum_{i=A, i\neq B}^{H} C_{i,cst} X_{i,9} + F_{11} \sum_{i=D}^{F} C_{i,cst} X_{i,11} + 0.0536 W_{\mathrm{cmp}} + 0.0318 F_{\mathrm{steam}}, \tag{3}$$

where F_9 and F_{11} are the molar flow rates (kmol h^{-1}) of Streams 9 and 11, respectively; $C_{i,cst}$ is the cost of Component i ($ $kmol^{-1}$) provided by [26]; $X_{i,j}$ represents the mole fraction of Component i in Stream j; W_{cmp} and F_{steam} are the compressor power (kW) and stripper steam flow rate (kg h^{-1}), respectively. The instantaneous off-specification cost (OSC) is defined as:

$$OSC(\$\,\mathrm{h}^{-1}) = \begin{cases} 0 & r - e \le \dfrac{x_G}{x_H} \le r + e, \\ F_{11}(X_{G,11}C_{G,cst} + X_{H,11}C_{H,cst}) & \text{Otherwise,} \end{cases} \tag{4}$$

where x_G and x_H are mass fractions of G and H in the product stream, respectively; r is the desired mass ratio of G/H, imposed by product quality requirements; and e is the tolerance within which the quality specification is considered satisfied. The parameters *r* and *e* were set to 1 (base case) and 0.03, respectively. If the G/H ratio falls outside the acceptable range, the product is off-specification and cannot be sold (assuming no further separation stages). Consequently, the money that would be earned by selling the products is counted as a loss.

The optimization is subject to lower and upper bounds X^L and X^U, respectively, on the decision variables, path constraints on some process variables (Subsection 3.3), and a closed-loop dynamic prediction model (Subsection 3.4).

It is noted that the DRTO formulation is flexible with respect to the choice of the objective function, e.g., by including control error in a weighted manner. The only limitation is that the reduced-order prediction model should be able to estimate and evaluate the objective function over the prediction horizon.

3.2. Decision variables

The control structure used in this study offers 11 free set points that can be taken as decision variables. The first operation mode, as defined in [26], is considered in this work. Therefore, the G/H mass ratio set point is fixed at 1. This leaves 10 set points for online optimization as considered in [28]. However, an equality constraint on the product flow is also enforced in [28], reducing the actual number of adjustable set points to 9. In this study, the set point for the mole fraction of E in the product is also excluded from the decision variables. The main reason for this is that the middle loop in the corresponding double-cascade configuration is a temperature control (Figure 1). The modeling of temperature requires energy equations, which are not considered in the nonlinear model developed in [38]. Therefore, the prediction model would not be able to predict the transient effects of the foregoing set point on the stripper temperature and steam consumption. For this reason, the set point for the mole fraction of E in the product is fixed at its optimal value in Mode 1, i.e., 0.58% [40]. Also, the recycle flow set point is not considered a decision variable because as will be discussed later, this variable is used as a manipulated variable in the closed-loop prediction model, and thus, is not available to the optimizer. The remaining 7 set points, as given in Table 1, are considered the decision variables and obtained from the DRTO.

Table 1. Decision variables of the DRTO.

3.3. Problem constraints

A number of constraints must be included in Problem (2) to ensure the plant operates safely and the key process variables are maintained within their desired bounds. The lower and upper bound constraints on the decision variables are given in Table 2. These bounds are set partly based on the alarm and shutdown limits on some key process variables as defined in [26]. To ensure these limits are not violated during the operation and in the face of disturbances, some safety margins are also considered for the more important set points such as the reactor pressure, temperature, and level. As stated in [40], the choice of the safety margins depends on the ability of the control structure to counteract disturbances. In this work, the safety margins are obtained according to the previous work on the TE process [26,28,31] and extensive simulations of the process. These margins are set conservatively such that the process can continue to operate safely despite possible overshoots caused by the control system. The set point bounds are implemented by simply setting lower and upper bounds on the decision variables.

Despite the presence of the set point bounds, the actual process variables evolve over time and may still go outside the safe or operable limits due to overshoots resulting from the process dynamics. To avoid such situations, path constraints on some of the key process variables are also enforced during the prediction horizon (see Table 3). The limits in Table 3 are for the most part the same as those given Table 2, except for (i) the reactor level, where the lower limit is set slightly lower than the set point's lower bound to account for possible undershoots caused by the control system and (ii) the reactor pressure, where the limits are set to the original shutdown limit given in [26] to allow for possible overshoots caused by the control system. The path constraints are not implemented for the reactor temperature as it cannot be predicted by the prediction model due to the lack of heat balances. Moreover, a parsimonious approach should be taken in adding new constraints as too many constraints could cause convergence difficulties for the large-scale nonlinear problem. Therefore, the path constraints are considered only for the variables that are critical to process stability, namely reactor pressure and the three liquid levels in the process. For simplicity, the path constraints are discretized and enforced at finite interior points over the prediction horizon [39,41]. In particular, they are enforced at every 0.2 h over the prediction horizon. As an example, the path constraint on reactor pressure $P_r(t)$ over the 1 h prediction is formulated as 5 constraints as

$P_r(0.2) \leq 3000$ kPa,

$P_r(0.4) \leq 3000$ kPa,

$P_r(0.6) \leq 3000$ kPa,

$P_r(0.8) \leq 3000$ kPa,

$P_r(1.0) \leq 3000$ kPa,

It is noted that Golshan et al. [28] used the reactor steady-state material balance as a nonlinear constraint. Nonetheless, this constraint is removed in this work because in contrast to conventional RTO, the objective function in DRTO is evaluated over a transient period. Therefore, the steady-state condition is not enforced in the DRTO.

Table 2. Bounds on the decision variables [26].

Table 3. Path constraints on predicted key process variables imposed over the prediction horizon.

3.4. Closed-loop prediction model

As part of the DRTO, a closed-loop prediction model is built to supply estimates of future outputs based on the trial set points and initial values of the states obtained from the current plant conditions. The prediction model consists of the TE nonlinear model [38] with a control system similar to the one implemented on the actual process However, it should be noted that it is not possible for the prediction model to implement exactly the same control structure used in the actual process. The reason is that the prediction model is a reduced-order model that lacks some details of the actual process. In particular, the model inputs are mostly flow rates of the streams, whereas the actual process inputs are mostly valve openings [26]. Therefore, the inner loops of the cascade structures that deal with the valve openings must be removed so that the flow rates can be manipulated directly in the model. The removal of the inner loops would not have a considerable impact on the model prediction owing to the fast dynamics between the valve percentage and flow rate. Moreover, the model ignores heat balance equations [38], and thus, may not behave in exactly the same way as the actual process, especially in case of temperature upsets. For example, it was observed that the dynamic model was too sensitive to changes to the separator and reactor temperatures, and the control system was not able to stabilize the model. The situation becomes more serious when the model starts from highly transient conditions. These differences between the nonlinear prediction model and the actual process call for some changes in the control structure or tunings so that the model can be stabilized and behave as similarly to the process as possible. Table 4 shows the control structure and tunings used in the prediction model. Due to the absence of heat balances in the model, any loops controlling the temperature had to be removed from the original control structure. These include the reactor outer and inner temperature controllers, the stripper temperature controller, and the condenser coolant's inner temperature controller. To compensate for the loss of control and reduce temperature sensitivity, concurrent loops were added to the reactor pressure and separator level by manipulating the E-feed flow and separator temperature, respectively. It is noted that the extra loops are proportional-only so they can merely play a stabilizing role without affecting the closed-loop response too much. Similarly, Ricker and Lee [42] had to stabilize the model used in their predictive control of the TE process by adding certain control loops to the model. The italicized variables and values in Table 4 represent the modifications made in this work.

Table 4. Loops and tuning parameters used for stabilization of the prediction model. Variables and values in italics represent the loops and tunings introduced/modified in this work.

Unless otherwise noted, the optimizer is executed every 1 h to obtain a new set of optimal set points. The prediction horizon is set to 1 h. Generally, longer prediction horizons could be used. However, integrating a rather large-scale nonlinear prediction model and enforcing path constraints over a longer time horizon would significantly increase the computational burden in terms of integration and optimization routines. In addition, the prediction model employed in this work is a reduced-order representation of the actual plant containing only mass balances. Therefore, the benefits of a longer prediction horizon may be offset by the accumulation of inaccuracies resulting from the model mismatch. Therefore, an 'ideal' prediction horizon would require a systematic analysis to find the trade-off between a longer prediction that could see a farther future and degraded prediction accuracy. Moreover, due to the system's nonlinearity, it can be argued that no single prediction horizon would remain ideal over the entire operation envelope.

Only one set of optimal set points (as opposed to a set point trajectory) is obtained at each DRTO execution. This choice is made to work around limited computational resources. A set point horizon of 2 or 3 would double or triple the number of decisions. This would increase the computational demand markedly, especially for a large-scale problem such as the TE process [43]. Despite the set point horizon of 1, the problem formulation solves a dynamic prediction model to optimize transient operating and off-specification costs subject to dynamic path constraints. Therefore, the proposed approach falls in the DRTO category regardless of the set point horizon and is distinct from conventional RTO.

4. Results and Discussions

The proposed strategy is applied to the TE process operating in the base case [26], where the production rate is supposed to remain close to 14076 kg/h (~ 23 m3/h) with a G/H ratio of 1. The algorithm could be adapted to work for operating conditions far from the base case (such as maximum capacity or turndown scenarios) by adding appropriate production constraints. Before doing so, however, the ability of the control system in maintaining the process stability and performance in extreme transient scenarios should be assessed. This is outside the scope of the DRTO algorithm.

Six scenarios are considered. In the first scenario, the process is operated without any disturbances. In the remaining five scenarios, five disturbances defined in [26] are introduced to the process during the operation. The successive quadratic programming (SQP) algorithm is employed for the optimization.

On a PC with Intel Core 3.2 GHz CPU and 16 GB RAM, the optimization at each RTO execution takes about 7 s and 0.02 s for the DRTO and conventional RTO, respectively. The large difference in the CPU times is expected for the following reasons: i) at each iteration of the optimization, DRTO solves a dynamic optimization problem that requires integrating the nonlinear dynamic model up to the prediction horizon; this is much more time-consuming than solving a steady-state model as in the conventional RTO, ii) due to the presence of path constraints, DRTO has more constraints to meet than the conventional RTO; therefore, it would generally require more iterations to converge. Despite the higher computational cost, the application of DRTO is justified as the CPU time is negligible considering the slow process dynamics (which takes hours to reach a steady state). Moreover, in real applications, the algorithm will be implemented as a fast executable program, rather than an interpreted program. It is worth noting that the use of PI loops in the regulatory is computationally advantageous over MPCs, which would add another optimization layer with a whole new set of model prediction and state estimation routines that would have to be run at every sample time. In order to compare the performance of the proposed DRTO with the conventional RTO [28], the actual total cost (as opposed to the predicted one) is defined based on the objective function in Problem (2) as

$$\begin{aligned} &\text{Total cost } (\$) = OC_{total} + OSC_{total}, \\ &OC_{total} \quad (\$) = \int_{t_0}^{t_f} OC_{plant}\, dt, \\ &OSC_{total} \ (\$) = \int_{t_0}^{t_f} OSC_{plant}\, dt, \end{aligned} \tag{5}$$

where OC_{plant} and OSC_{plant} are the actual instantaneous plant operating cost and off-specification cost, respectively. The actual total cost is obtained by integrating the sum of the two costs from the first optimizer execution (t_0) to the end of the simulation (t_f). In all the simulations, t_0 is set to 10 h, i.e., the time at which the plant is nominally steady after an initial transient period. Also, t_f is set to 90 h, up to which the process is expected to reach a new steady state. It is noted that the RTO proposed in [28] is also rerun with a frequency of every 1 h in order to have a meaningful comparison with the present work. The cost difference between DRTO and conventional RTO stems from their treatment of process transitions. While conventional RTO optimizes only the steady-state cost, DRTO evaluates the cumulative cost over the prediction horizon, including transient operating inefficiencies and off-specification product losses. This leads to more economically favorable transitions and improves overall performance, especially under disturbances.

The model of the TE process is integrated using the fixed-step size method Bogacki-Shampine with a sample time of 0.001 h. The numerical results for each scenario are discussed in the following subsections.

4.1. Economic performance under normal operation

In this case, the TE process is operated in the absence of disturbances. It is worth noting that even in the absence of disturbances, the DRTO must deal with stochastic measurement noise and parametric and structural uncertainties resulting from the plant-model mismatch. As shown in Table 5, the proposed DRTO reduces the total cost ($) by 4.4% compared with the conventional RTO in this case. Interestingly, the steady-state operating cost ($\$ h^{-1}$) at the new steady state is quite the same as that obtained from the conventional RTO in [28].

4.2. Economic performance under disturbances

Five scenarios involving sustained disturbances (also referred to as IDV) are presented in this subsection. The disturbance used in each scenario is given in Table 6. The choice of the disturbances seems practical as the feed ratio, composition, and temperature are common unwanted upsets in chemical processes. In each disturbance scenario, the disturbance of interest becomes active after 10 h of the plant operation, lasting until the end of the simulation. The activation time coincides with the first execution of the (D)RTO strategy.

In Scenario 2, in which IDV_1 is active, the DRTO strategy reduces the total cost by 28.2%, which is a significant saving. As shown in Table 5, this saving is mainly due to reducing the total off-specification cost, which means that the product quality is better maintained within the desired specification during the transition. Figure 3 illustrates the G/H ratio variations for the proposed DRTO versus that for the conventional RTO [28]. The horizontal dotted grid lines show the acceptable product quality interval between 1.03 and 0.97. As shown in Figure 3, the G/H ratio for the proposed DRTO violates the desired specification less frequently compared with the conventional RTO, resulting in considerable saving in the off-specification production cost. Although the objective function is the sum of the total operating and total off-specification costs, the total operating cost in DRTO is almost the same as, and in some cases, even slightly higher than that in the conventional RTO (Table 5). The reason for this is that the total off-specification product cost is an order of magnitude greater than the total operating cost, thereby dominating the value of the objective function. Consequently, any attempt to minimize the objective function would have a greater effect on the total off-specification product cost than on the total operating cost.

Figure 3. On-specification production of the proposed DRTO compared with that of the conventional RTO [28] when IDV_1 is active; acceptable G/H ratio is defined by the red dashed lines.

When IDV_2 is active in the third scenario, the proposed DRTO yields saving of 9.4% in the total cost (Table 5). This scenario shows how the optimization strategy makes a tradeoff between the operating cost and the off-specification cost so as to minimize the whole objective function.

Figure 4. Operating cost during optimization when IDV_2 is active for the proposed DRTO.

Figure 5. Operating cost during optimization when IDV_2 is active for the conventional RTO [28].

The instantaneous operating costs from the third scenario are shown in Figures 4-5. Figure 4 shows the operating cost ($ h^{-1}) obtained from the proposed DRTO. It can be seen that the instantaneous operating cost increases considerably (to above 240 $ h^{-1}) over a short period in the DRTO case. It then decreases to below 160 $ h^{-1} before it settles to its steady state value. Figure 5 shows the operating cost obtained from the conventional RTO [28], where a relatively uniform trend is observed. From Table 5, the total operating cost ($) in the DRTO case is about 2% higher than that in the conventional RTO. On the other hand, the off-specification cost in the DRTO case is 25% lower than that in the conventional RTO. This verifies that the operating and off-specification costs can be conflicting objectives, where an increase in one can result in a decrease in the other, justifying the multi-objective optimization considered in Problem (2).

From Table 5, it is interesting to see that the total transient cost has decreased by 9.4% compared with the conventional RTO. This shows that the temporary increase in the DRTO operating cost (Figure 4) has a positive effect on the total cost overall. The saving is achieved by reducing the off-specification production as discussed above. From Figures 4-5 and Table 5, it can be seen that IDV_2 leaves a remarkable effect on the steady-state operating cost, which seems to be the minimum achievable for the third scenario. Interestingly, the instantaneous operating cost ($ h^{-1}) in the new steady state is almost the same for both DRTO and RTO. Therefore, the DRTO will not impose extra costs to the long-term plant operation.

In Scenarios 4 to 6, temperature disturbances are introduced to the process. In Scenario 4 with IDV_3 being activated, a saving of 5.3% over the conventional RTO is achieved (Table 5). Figures 6-7 show key process variables for both DRTO and RTO strategies under Scenario 4. The liquid levels in the reactor, separator, and stripper have a noticeably different trajectory between the RTO and proposed DRTO strategies. These variables represent the process liquid inventories, and serve as a buffer capacity in case of process disturbances. Therefore, it appears that the DRTO exploits this buffer capacity to counteract the adverse effects of the step change in the D feed temperature (IDV_3).

In Scenario 5 with IDV_4 being activated, the saving is 4.3%. In Scenario 6, IDV_5 is activated. In Scenario 6a, the DRTO is executed every 1 hour, as in the previous scenarios. As seen in Table 5, DRTO results in a saving of about 3% over the conventional RTO in this case.

Figure 6. Key process variables when IDV_3 is active for the proposed DRTO.

Figure 7. Key process variables when IDV_3 is active for the conventional RTO [28].

For the reasons mentioned previously, the DRTO prediction has been kept short (i.e., 1 h) in the case studies shown thus far. Therefore, the prediction and control horizons have been the same. In order to investigate the potential positive effects of a longer prediction horizon, the DRTO can be executed more frequently than every 1 hour. In particular, it is executed every 30 min in Scenario 6b. By doing so, the prediction horizon of 1 h becomes twice as long as the control horizon (i.e., 30 min). As a result, the effects of unequal prediction and control horizons can be assessed without having to increase the prediction horizon and potentially accumulating plant-model mismatch inaccuracies. The total cost from DRTO in Scenario 6b is 6% lower than that from the conventional RTO. This compared with the 3% improvement over conventional RTO in Scenario 6a would confirm the common understanding that longer prediction horizons can generally improve the results. In fact, a longer prediction horizon, or in a sense, more frequent optimization reduces the total cost from 42215 ($) to 40858 ($) in the proposed DRTO. In Figures 8-9, the accumulation of the actual off-specification cost and total cost with time is compared for all the cases run in Scenario 6. The off-specification cost (Figure 8) increases only when the product G/H ratio goes outside the acceptable limit and is constant otherwise. On the other hand, the total cost (Figure 9) has an ever-increasing trend because the operating cost portion of it is always non-zero regardless of the product quality. During the off-specification production, the total cost takes a steeper slope consistent with the off-specification cost in Figure 8. The cost calculations start upon the first optimization trigger at t=10 h.

It can be checked from Table 5 that the total off-specification cost constitutes about 70% of the total transient cost on average, justifying its inclusion in the DRTO objective function. It is also worth noting that in all the scenarios, the DRTO approach yields virtually the same steady-state OC ($ h^{-1}) as the conventional RTO. The DRTO results in a slightly (up to about 3%) lower OC in some scenarios and a negligibly higher OC in the others. The differences between the two approaches are too small to be important and can be attributed to the optimization routine or the effect of process noises on the cost function variations. In fact, it would be expected for the two approaches to yield the same steady-state OC in the scenarios studied here. Specifically, in all the scenarios, the process will eventually reach a steady state because either there is no disturbance or there is a sustained stepwise disturbance. In the new steady state, the product will be naturally on-specification owing to the PI controller for the product G/H ratio (Figure 1), provided the corresponding valve is not saturated. Therefore, the off-specification cost will be zero in the new steady state. As a result, the total OC ($) and OC ($ h^{-1}) are the only terms that remain and are minimized in, respectively, the DRTO and RTO cost functions after the transient period.

Table 5. Results of the proposed DRTO against those obtained by the conventional RTO in [28]. The percentage saved is based on the total transient cost for both strategies. Scenario 6b is the same as Scenario 6b with the DRTO executed every 30 min.

Table 6. Disturbances used in the last five scenarios.

Figure 8. The accumulation of the off-specification cost over time for the conventional RTO, DRTO with execution interval of 1 h, and DRTO with execution interval of 30 min in Scenario 6.

Figure 9. The accumulation of the total cost over time for the conventional RTO, DRTO with execution interval of 1 h, and DRTO with execution interval of 30 min in Scenario 6.

5. Conclusion

A DRTO strategy considering both transient off-specification and operating costs has been developed for the TE process for the first time. Unlike smaller processes often considered in the previous DRTO studies, the TE process is a relatively large-scale benchmark with high dynamic interactions. It is also open-loop unstable, precluding the use of open-loop prediction models as employed in many previous RTO work. To resolve this issue, a closed-loop prediction model has been developed for the DRTO, as advocated in more recent DRTO studies. The closed-loop prediction and optimization in this work is expected to be more robust and less expensive than the previous CL-DRTO efforts owing to the use of PI controllers instead of MPC. The use of PI controllers together with the enforcement of bounds on the optimal set points ensure closed-loop stability of the DRTO in case of potential conflicts between the economic and control tracking objectives. A major challenge in the application of DRTO to large-scale processes is the lack of a high-fidelity dynamic prediction model, as rigorous modeling can prove to be hard or impossible for large-scale systems with complicated phenomena. While a reduced-order model is employed for prediction in this work, the use of a rigorous model would yield improved results theoretically. However, it should be noted that the computational cost would grow substantially with a rigorous model. Although model linearization can reduce computational burden, as is common in MPC, it is not recommended in DRTO applications. Since the prediction horizon in DRTO is considerably longer, a linearized model may deviate significantly from the actual process behavior over a long horizon. Therefore, the challenge of a prediction model with sufficient fidelity that allows for hours of prediction, and at the same time, is computationally inexpensive to optimize remains to be addressed before DRTO becomes a viable tool for industrial applications.

References

[1] Pantelides, C.C., Pereira, F.E., Stanger, P.J., et al., "Process operations: from models and data to digital applications", *Comput. Chem. Eng.*, **180**, 108463 (2024). https://doi.org/10.1016/J.COMPCHEMENG.2023.108463.

[2] Wang, Z., Yu, D., Wu, Z., "Real-time machine-learning-based optimization using Input Convex Long Short-Term Memory network", *Appl. Energy,* **377**, 124472 (2025). https://doi.org/10.1016/J.APENERGY.2024.124472.

[3] Krishnamoorthy, D., Doyle, F.J., "Model-free real-time optimization of process systems using safe Bayesian optimization", *AIChE J.*, **69,** e17993 (2023). https://doi.org/10.1002/AIC.17993.

[4] de Azevedo Delou, P., Matias, J., Jäschke, J., et al., "Steady-state real-time optimization using transient measurements and approximated Hammerstein dynamic model: A proof of concept in an experimental rig", *J. Process Control*, **132**, 103111 (2023). https://doi.org/10.1016/J.JPROCONT.2023.103111.

[5] Forbes, J.F., Marlin, T.E., "Model accuracy for economic optimizing controllers: The bias update case", *Ind. Eng. Chem. Res*., **33**, 1919–1929 (1994). https://doi.org/10.1016/0140-6701(95)93809-5.

[6] Raven, D.B., Chikkula, Y., Patel, K.M., et al., "Machine learning & conventional approaches to process control & optimization: Industrial applications & perspectives", *Comput. Chem. Eng*., **189**, 108789 (2024). https://doi.org/10.1016/J.COMPCHEMENG.2024.108789.

[7] Zhu, Y., Yang, C., Chen, X., et al., "Identification-based real-time optimization and its application to power plants", *Control Eng. Pract*., **123**, 105160 (2022). https://doi.org/10.1016/J.CONENGPRAC.2022.105160.

[8] MacKinnon, L., Swartz, C.L.E., "Robust closed-loop dynamic real-time optimization", *J. Process Control*, **126**, 12–25 (2023). https://doi.org/10.1016/J.JPROCONT.2023.04.003.

[9] Yan, P., Bai, M., Cai, X., et al., "Data-driven dynamic optimization for real-time parking reservation considering parking unpunctuality", *IISE Trans*., **57**, 90–103 (2025). https://doi.org/10.1080/24725854.2023.2286631.

[10] Zhang, Z., Wu, Z., Rincon, D., et al., "Real-Time Optimization and Control of Nonlinear Processes Using Machine Learning", *Mathematics*, **7**, 890 (2019) 890. https://doi.org/10.3390/MATH7100890.

[11] Galan, A., de Prada, C., Gutierrez, G., et al., "Implementation of RTO in a large hydrogen network considering uncertainty", *Optim. Eng*., **20**, 1161–1190 (2019). https://doi.org/10.1007/S11081-019-09444-3.

[12] Krishnamoorthy, D., Skogestad, S., "Real-Time optimization as a feedback control problem – A review", *Comput. Chem. Eng*., **161**, 107723 (2022). https://doi.org/10.1016/j.compchemeng.2022.107723.

[13] Thierry, D., Biegler, L.T., "Dynamic real-time optimization for a CO2 capture process", *AIChE J*., **65**, e16511 (2019). https://doi.org/10.1002/AIC.16511.

[14] Rossi, F., Rovaglio, M., Manenti, F., "Model predictive control and dynamic real-time optimization of steam cracking units", *Comput. Aided Chem. Eng*., **45**, 873–897 (2019). https://doi.org/10.1016/B978-0-444-64087-1.00018-8.

[15] Jung, H., Kim, J.W., Lee, J.M., "Two-stage dynamic real-time optimization framework using parameter-dependent differential dynamic programming", *Comput. Chem. Eng*., **192**, 108896 (2025).

https://doi.org/10.1016/J.COMPCHEMENG.2024.108896.
[16] Jamaludin, M.Z., Swartz, C.L.E., "Approximation of closed-loop prediction for dynamic real-time optimization calculations", *Comput. Chem. Eng.*, **103**, 23–38 (2017). https://doi.org/10.1016/j.compchemeng.2017.02.037.
[17] Jamaludin, M.Z., Swartz, C.L.E., "Dynamic Real-Time Optimization with Closed-Loop Prediction", *AIChE J.*, **63**, 3896–3911 (2017). https://doi.org/10.1002/aic.
[18] Bonvin, D., Srinivasan, B., "On the role of the necessary conditions of optimality in structuring dynamic real-time optimization schemes", *Comput. Chem. Eng.*, **51**, 172–180 (2013). https://doi.org/10.1016/J.COMPCHEMENG.2012.07.012.
[19] Ramesh, P.S., Swartz, C.L.E., Mhaskar, P., "Closed-loop dynamic real-time optimization with stabilizing model predictive control", *AIChE J.*, **67**, 1–35 (2021). https://doi.org/10.1002/aic.17308.
[20] Kim, R., Lima, F. V., "Nonlinear multiobjective and dynamic real-time predictive optimization for optimal operation of baseload power plants under variable renewable energy", *Optim. Control Appl. Methods*, **44**, 798–829 (2023). https://doi.org/10.1002/oca.2852.
[21] Bousbia-Salah, R., Florez, D., Lesage, F., et al., "Grafting of Styrene on Ground Tire Rubber Particles in a Batch Polymerization Reactor: Dynamic Real-Time Optimization", *Ind. Eng. Chem. Res.*, **58**, 13622–13627 (2019). https://doi.org/10.1021/ACS.IECR.9B00738.
[22] Untrau, A., Sochard, S., Marias, F., et al., "Analysis and future perspectives for the application of Dynamic Real-Time Optimization to solar thermal plants: A review", *Sol. Energy*, **241**, 275–291 (2022). https://doi.org/10.1016/J.SOLENER.2022.05.058.
[23] Xu, H., Zhang, A., Wang, Q., et al., "Quantum Reinforcement Learning for real-time optimization in Electric Vehicle charging systems", *Appl. Energy*, **383**, 125279 (2025). https://doi.org/10.1016/J.APENERGY.2025.125279.
[24] MacKinnon, L., Ramesh, P.S., Mhaskar, P., et al., "Dynamic real-time optimization for nonlinear systems with Lyapunov stabilizing MPC", *J. Process Control*, **114**, 1–15 (2022). https://doi.org/10.1016/J.JPROCONT.2022.03.009.
[25] Pataro, I.M.L., da Costa, M.V.A., Joseph, B., "Closed-loop dynamic real-time optimization (CL-DRTO) of a bioethanol distillation process using an advanced multilayer control architecture", *Comput. Chem. Eng.*, **143**, 107075 (2020). https://doi.org/10.1016/J.COMPCHEMENG.2020.107075.
[26] Downs, J.J., Vogel, E.F., "A plant-wide industrial process control problem", *Comput. Chem. Eng.*, **17**, 245–255 (1993). https://doi.org/10.1016/0098-1354(93)80018-I.
[27] Jockenhövel, T., Biegler, L.T., Wächter, A., "Dynamic optimization of the Tennessee Eastman process using the OptControlCentre", *Comput. Chem. Eng.*, **27**, 1513–1531 (2003). https://doi.org/10.1016/S0098-1354(03)00113-3.
[28] Golshan, M., Boozarjomehry, R.B., Pishvaie, M.R., "A new approach to real time optimization of the Tennessee Eastman challenge problem", *Chem. Eng. J.*, **112**, 33–44 (2005). https://doi.org/10.1016/j.cej.2005.06.005.
[29] Golshan, M., Pishvaie, M.R., Boozarjomehry, R.B., "Stochastic and global real time optimization of Tennessee Eastman challenge problem", *Eng. Appl. Artif. Intell.*, **21**, 215–228 (2008). https://doi.org/10.1016/j.engappai.2007.04.004.
[30] Golshan, M., Boozarjomehry, R.B., Sahlodin, A.M., et al., "Fuzzy real-time

optimization of the Tennessee Eastman challenge process", *Iran. J. Chem. Chem. Eng*., **30**, 31–43 (2011).
[31] Duvall, P.M., Riggs, J.B., "On-line optimization of the Tennessee Eastman challenge problem", *J. Process Control*, **10**, 19–33 (2000). https://doi.org/10.1016/S0959-1524(99)00041-4.
[32] Papasavvas, A., Francois, G., "Internal Modifier Adaptation for the Optimization of Large-Scale Plants with Inaccurate Models", *Ind. Eng. Chem. Res*., **58**, 13568–13582 (2019). https://doi.org/10.1021/ACS.IECR.9B00246.
[33] Villagómez, E.L., Mahalec, V., "Fault detection and identification using a novel process decomposition algorithm for distributed process monitoring", *J. Process Control*, **149**, 103423 (2025). https://doi.org/10.1016/j.jprocont.2025.103423.
[34] Zhao, S., Duan, Y., Roy, N., et al., "A novel fault diagnosis framework empowered by LSTM and attention: A case study on the Tennessee Eastman process", *Can. J. Chem. Eng*., **103**, 1763 (2025). https://doi.org/10.1002/cjce.25460.
[35] Shaik, A.K., Das, A., Palleti, V.R., "Adversarial attacks on anomaly detectors in process systems: A case study on Tennessee Eastman process dataset", *Can. J. Chem. Eng*., **104**, 3068-3102 (2026). https://doi.org/10.1002/CJCE.70202.
[36] McAvoy, T.J., Ye, N., "Base control for the Tennessee Eastman problem", *Comput. Chem. Eng*., **18**, 383–413 (1994). https://doi.org/10.1016/0098-1354(94)88019-0.
[37] Miao, A., Tao, F., Li, P., et al., "An improved Fisher discriminant analysis algorithm based on Procrustes analysis for adaptive fault recognition", *Meas. Control*, **52**, 1063–1071 (2019). https://doi.org/10.1177/0020294019858103.
[38] Ricker, N.L., Lee, J.H., "Nonlinear modeling and state estimation for the Tennessee Eastman challenge process", *Comput. Chem. Eng*., **19**, 983–1005 (1995). https://doi.org/10.1016/0098-1354(94)00113-3.
[39] Chachuat, B., "Nonlinear and Dynamic Optimization: From Theory to Practice", *Polycopiés l'EPFL*, EPFL (2009).
[40] Ricker, N.L., "Optimal steady-state operation of the Tennessee Eastman challenge process", *Comput. Chem. Eng*., **19**, 949–959 (1995). https://doi.org/10.1016/0098-1354(94)00043-N.
[41] Vassiliadis, V.S., Sargent, R.W.H., Pantelides, C.C., "Solution of a Class of Multistage Dynamic Optimization Problems. 2. Problems with Path Constraints", *Ind. Eng. Chem. Res*, **33**, 2123–2133 (1994).
[42] Ricker, N.L., Lee, J.H., "Nonlinear model predictive control of the Tennessee Eastman challenge process", *Comput. Chem. Eng*., **19**, 961–981 (1995). https://doi.org/10.1016/0098-1354(94)00105-W.
[43] Yan, M., Multi-objective, "Plant-wide control and optimization of chemical processes", University of Washington (1996).

List of figure captions

Figure 1	The Tennessee Eastman process and its control system [26,36]; figure taken and adapted from the open-access article [37].
Figure 2	Proposed DRTO procedure.
Figure 3	On-specification production of the proposed DRTO compared with that of the conventional RTO [28] when IDV_1 is active; acceptable G/H ratio is defined by the red dashed lines.
Figure 4	Operating cost during optimization when IDV_2 is active for the proposed DRTO
Figure 5	Operating cost during optimization when IDV_2 is active for the conventional RTO [28]
Figure 6	Key process variables when IDV_3 is active for the proposed DRTO.
Figure 7	Key process variables when IDV_3 is active for the conventional RTO [28].
Figure 8	The accumulation of the off-specification cost over time for the conventional RTO, DRTO with execution interval of 1 h, and DRTO with execution interval of 30 min in Scenario 6.
Figure 9	The accumulation of the total cost over time for the conventional RTO, DRTO with execution interval of 1 h, and DRTO with execution interval of 30 min in Scenario 6.

List of table captions

Table number	Caption
Table 1.	Decision variables of the DRTO.
Table 2.	Bounds on the decision variables [26].
Table 3.	Path constraints on predicted key process variables imposed over the prediction horizon.
Table 4.	Loops and tuning parameters used for stabilization of the prediction model. Variables and values in italics represent the loops and tunings introduced/modified in this work.
Table 5.	Results of the proposed DRTO against those obtained by the conventional RTO in [28]. The percentage saved is based on the total transient cost for both strategies. Scenario 6b is the same as Scenario 6b with the DRTO executed every 30 min.
Table 6.	Disturbances used in the last five scenarios.

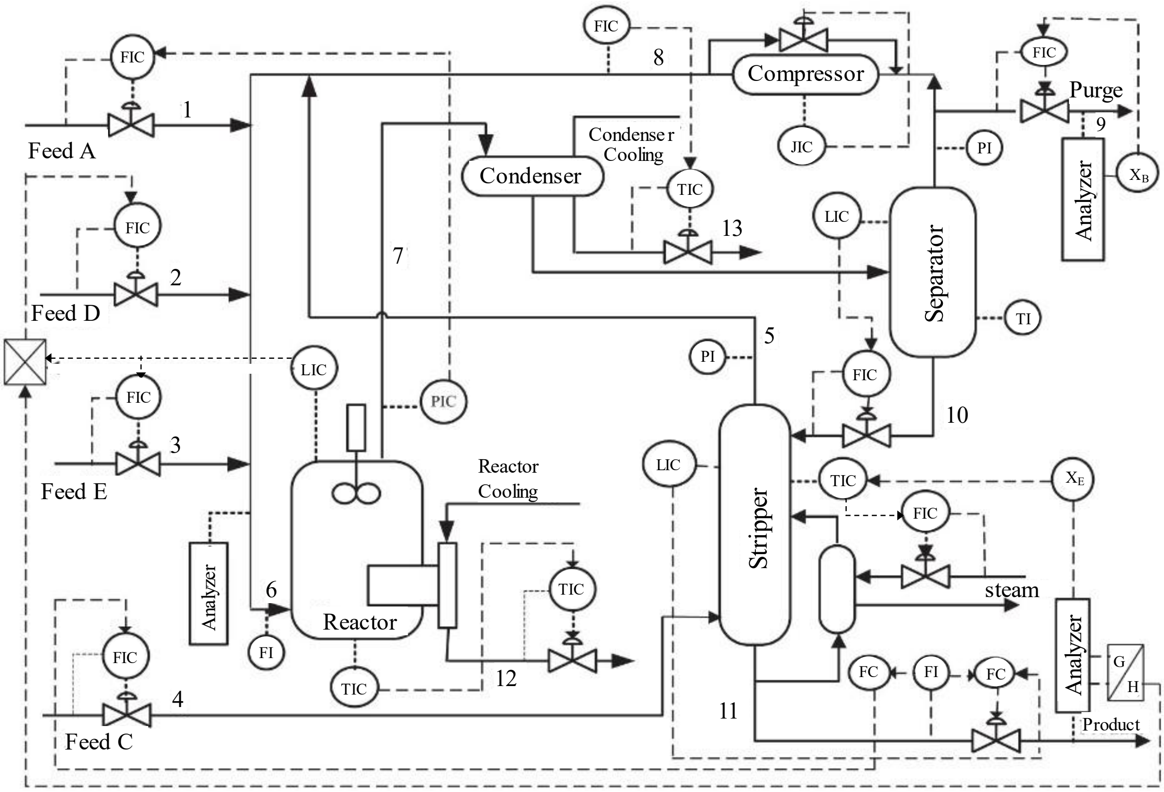
FIC
8
Compressor
FIC
Purge
9
1
Feed A
Condenser Cooling
JIC
PI
Condenser
TIC
Analyzer
XB
FIC
13
LIC
2
7
Separator
Feed D
TI
5
LIC
PI
FIC
FIC
PIC
10
3
Reactor Cooling
LIC
TIC
XE
Feed E
FIC
Stripper
Analyzer
TIC
steam
6
Reactor
Analyzer
FI
FIC
FC
FI
FC
G
H
4
TIC
12
Feed C
11
Product

Figure 1

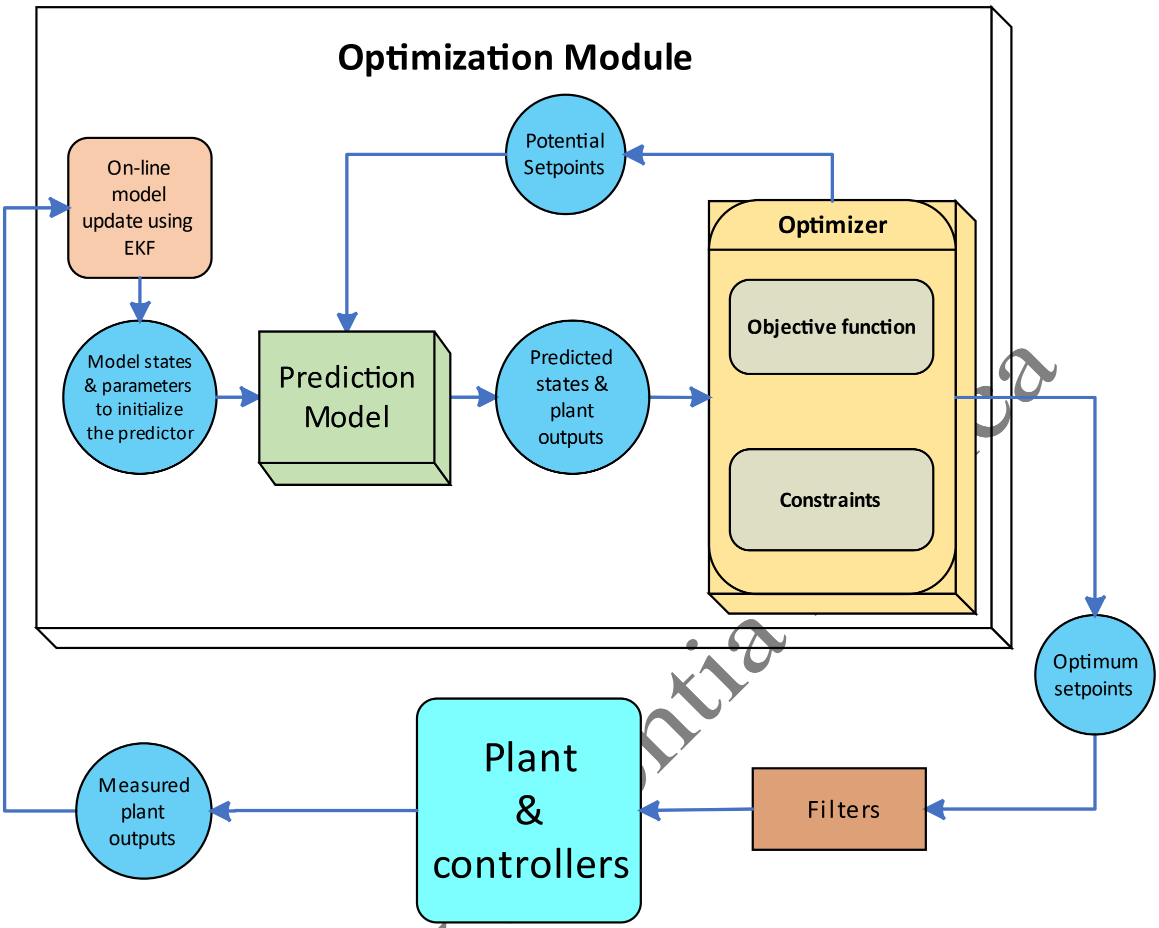

Optimization Module
Potential Setpoints
On-line model update using EKF
Optimizer
Objective function
Model states & parameters to initialize the predictor
Prediction Model
Predicted states & plant outputs
Constraints
Optimum setpoints
Plant & controllers
Measured plant outputs
Filters

Figure 2

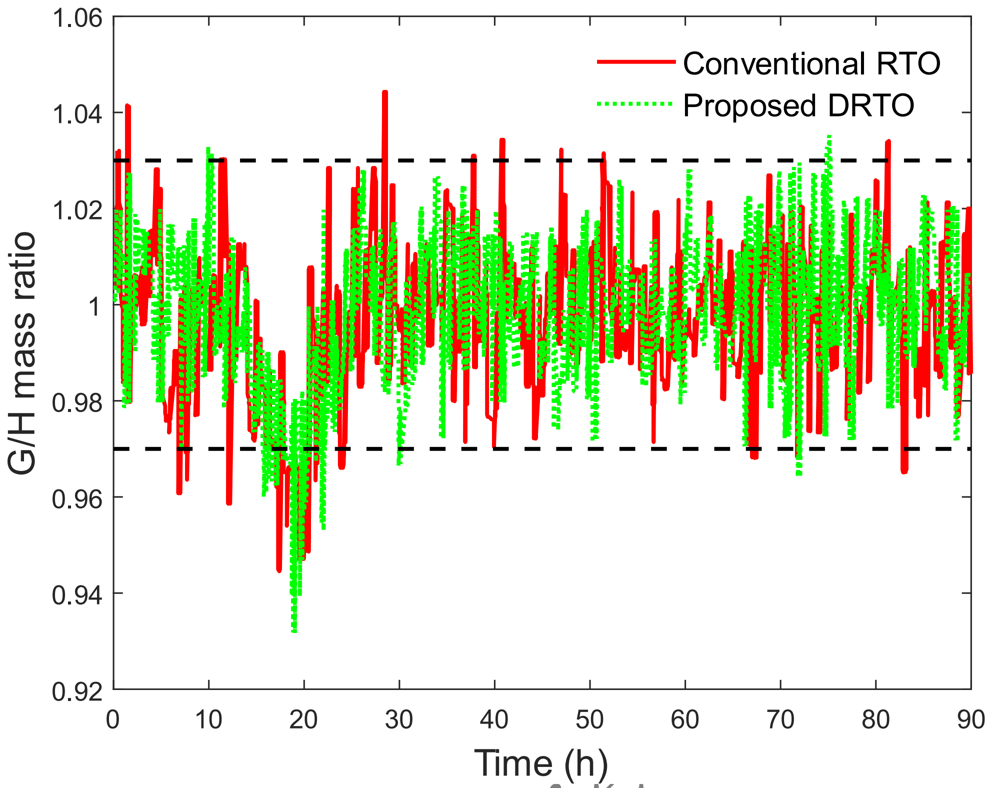

Figure 3

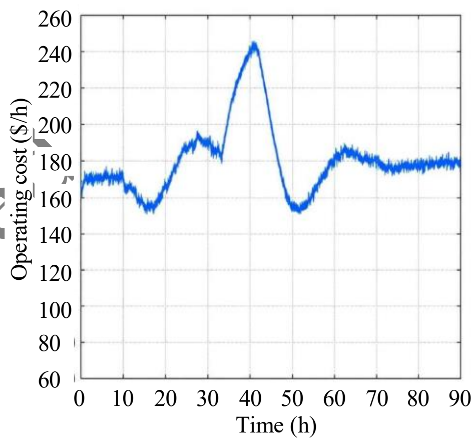

Figure 4

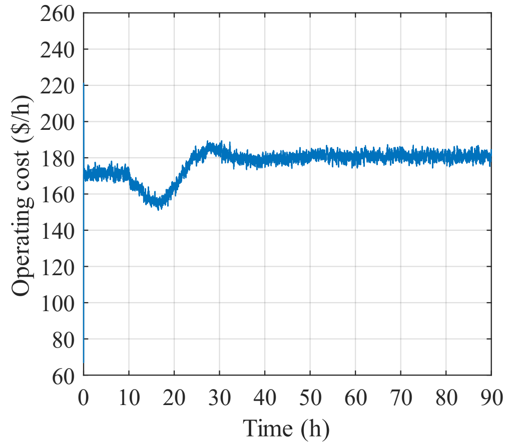

Figure 5

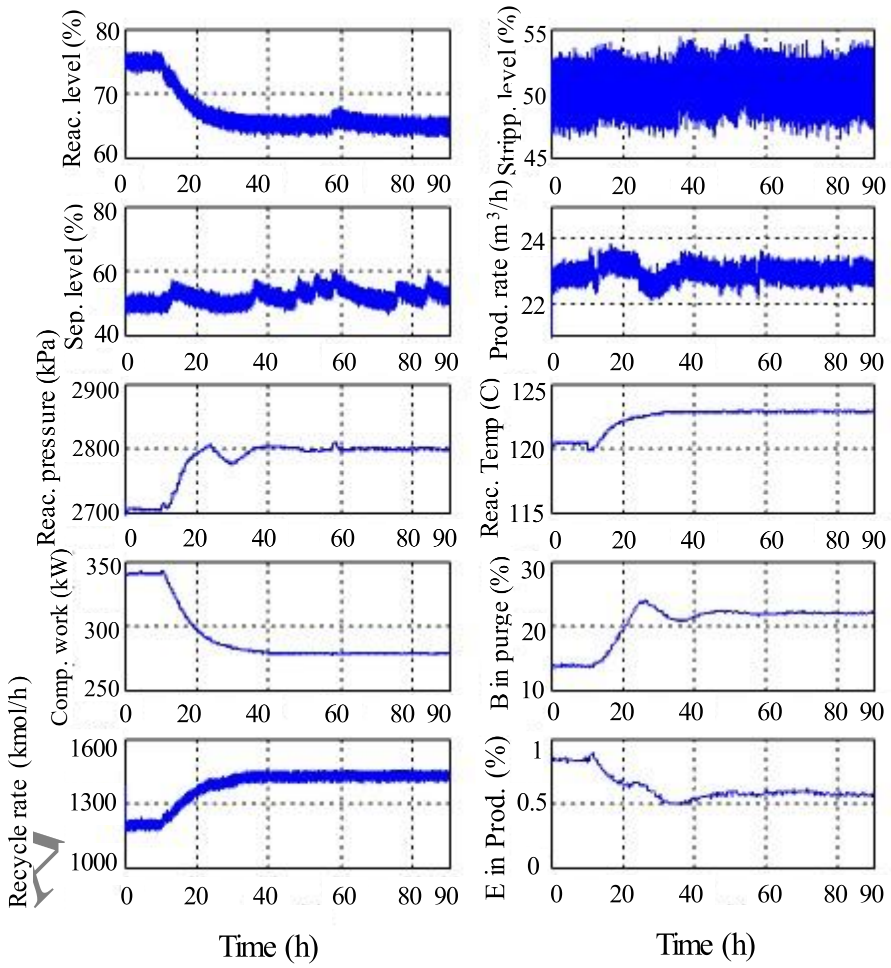

Figure 6

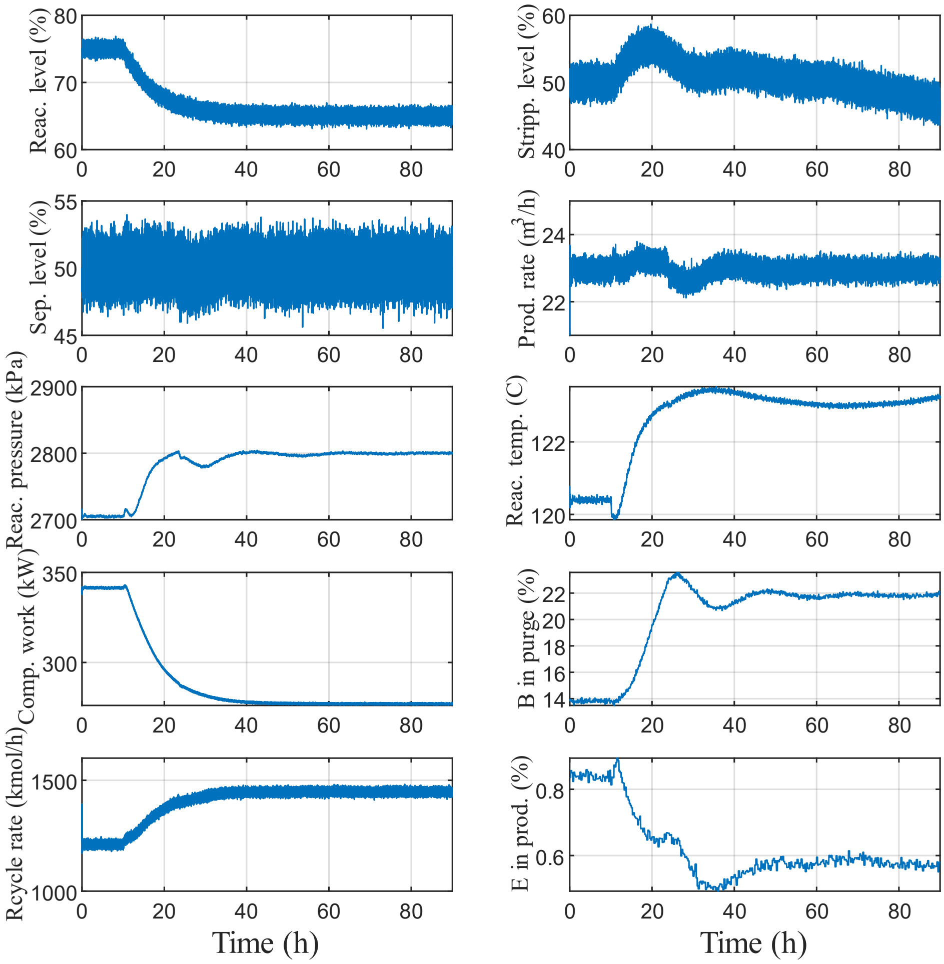
Reac. level (%)
Stripp. level (%)
Sep. level (%)
Prod. rate (m3/h)
Reac. pressure (kPa)
Reac. temp. (C)
Comp. work (kW)
B in purge (%)
Rcycle rate (kmol/h)
E in prod. (%)
Time (h)
Time (h)

Figure 7

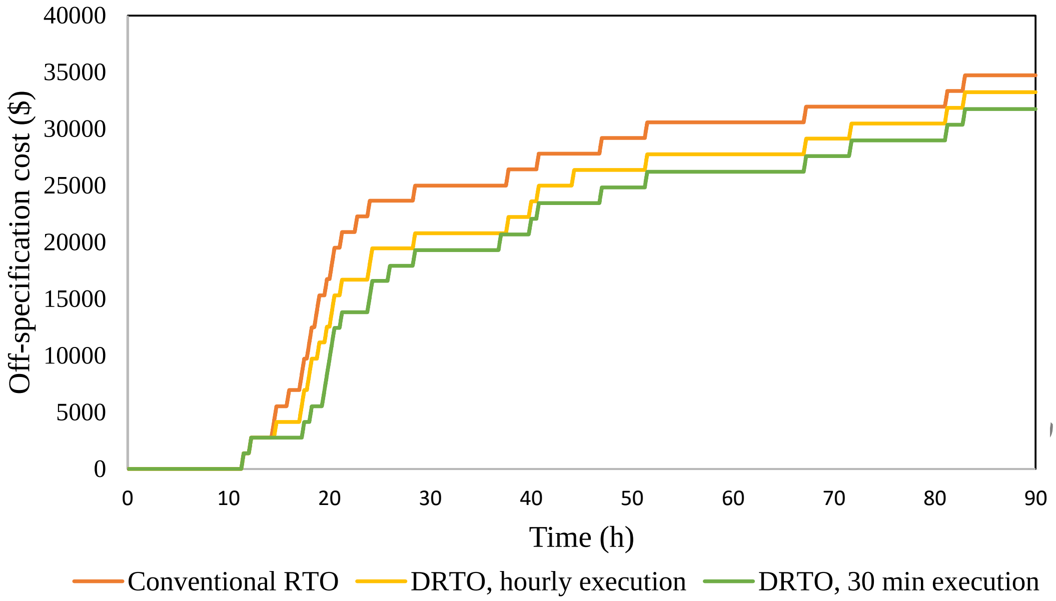

Figure 8

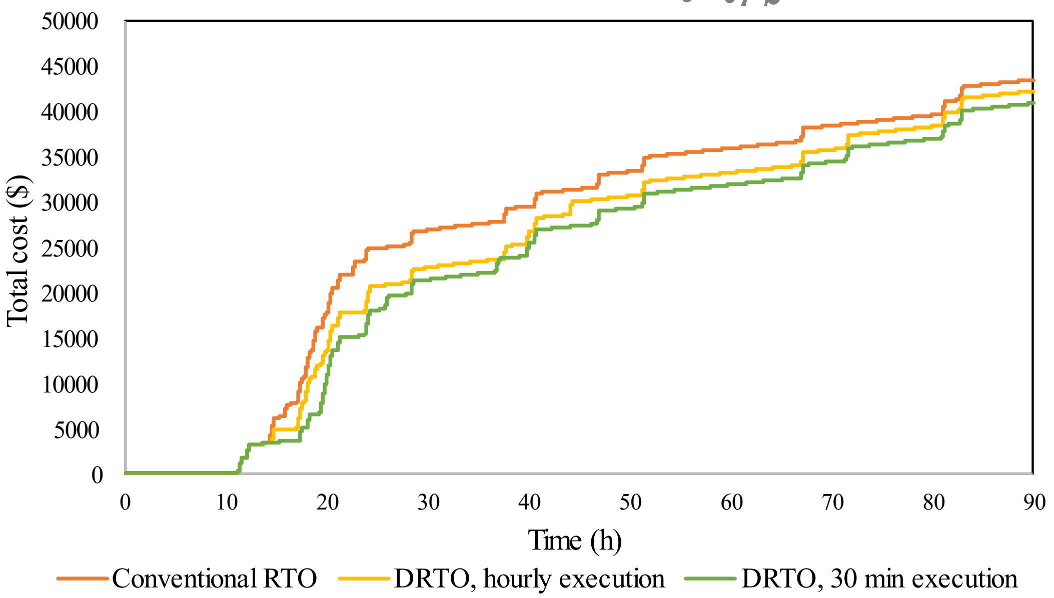

Figure 9

Table 1

Variable number	Variable name
1	Reactor level set point
2	Stripper level set point
3	Separator level set point
4	Reactor pressure set point
5	Reactor temperature set point
6	Compressor power set point
7	B% in purge set point

Table 2

Decision variable	Lower bound	Upper bound
Reactor pressure set point (kPa)	2700	2850
Reactor temperature set point (C)	118	124
Reactor level set point (%)	55	80
Separator level set point (%)	30	80
Stripper level set point (%)	30	80
B% in purge set point	10	22
Compressor work set point (kW)	277	360

Table 3

Process variable	Lower bound	Upper bound
Reactor pressure (kPa)	-	3000
Reactor level (%)	50	80
Separator level (%)	30	80
Stripper level (%)	30	80

Table 4

Controlled variable	Manipulated variable	Controller gain (K_c)	Integral time (τ_i, min)
Reactor pressure	A-feed flow	-0.143 (kmol/h kPa^{-1})	300
	E-feed flow	*1* (kmol/h kPa^{-1})	-
Reactor level	*Recycle flow*	*-250* (kmol/h %$^{-1}$)	*150*
Separator level	Separator underflow	*-3.36* (kmol/h %$^{-1}$)	*60*
	Separator temperature	*-5* (^{0}C %$^{-1}$)	-
Stripper level	Product flow	*-0.91* (kmol/h %$^{-1}$)	*60*
Mol fraction of B in purge	Purge rate	-1.34 (kmol/h %$^{-1}$)	100
Product G/H ratio	D/E feed ratio	0.05	40
Product flow	C-feed flow	3.57 (kmol m^{-3})	*40*

Table 5

		Golshan et al. [28]				Present work				
Scenario	Description	Total cost ($)	OC_{total} ($)	OSC_{total} ($)	Steady state OC ($ h^{-1})	Total cost ($)	OC_{total} ($)	OSC_{total} ($)	Steady state OC ($ h^{-1})	Percentage saved (%)
1	No disturbance	**32239**	8663	23575	115.8	**30834**	8691	22143	116.4	***4.4***

2	IDV 1	**44828**	8508	36317	117.12	**32187**	8506	23680	114.03	***28.2***
3	IDV 2	**25248**	14214	11033	183.7	**22864**	14561	8303	182	***9.4***
4	IDV 3	**51745**	8677	43068	116.5	**49022**	8711	40311	116.9	***5.3***
5	IDV 4	**32240**	8667	23572	116.3	**30845**	8690	22155	116.7	***4.3***
6a	IDV 5	**43462**	8724	34738	117	**42215**	8945	33270	118.9	***2.9***
6b	IDV 5	The same as above				**40858**	9118	31740	118.8	***6.0***

Table 6

Scenario	IDV	Description	Type
2	1	A/C feed ratio, B composition constant (stream 4)	Step
3	2	B composition, A/C ratio constant (stream 4)	Step
4	3	D feed temperature (stream 2)	Step
5	4	Reactor cooling water inlet temperature	Step
6	5	Condenser cooling water inlet temperature	Step

Biography

Ali Mohammad Sahlodin is an assistant professor of chemical engineering at Amirkabir University of Technology. He received his BSc, MSc, and PhD from the University of Tehran (2005), Sharif University of Technology (2007), and McMaster University (2012), respectively. He was a postdoctoral associate at Massachusetts Institute of Technology from 2013 to 2015 and worked as a senior R&D engineer at Aspen Technology from 2016 to 2018. His main research interests include advanced process control, dynamic simulation, and optimization under uncertainty with applications to process integration and intensification, especially water and CO2 minimization.

Ramin Bozorgmehry Boozarjomehry received MS and PhD degrees in Chemical Engineering from Sharif University of Technology (SUT), Tehran, Iran, and the University of Calgary, Canada, in 1990 and 1997, respectively. He is currently Professor in the Chemical & Petroleum Engineering Department at SUT. He has also worked at Hyprotech Ltd., in various software development projects. His research interests include application of AI in chemical engineering, modeling & simulation of novel systems, and control and optimization of nonlinear systems.

Mohammad Fakhroleslam received his BSc (2010) and MSc (2012) from Sharif University of Technology, and PhD (2017) from the University of Tehran, all in Chemical Engineering. He is an Associate Professor of Chemical Engineering at Tarbiat Modares University, with research expertise in process and energy systems engineering, value chain analysis in the oil, gas, and petrochemicals industries, and application of artificial intelligence in chemical engineering. He was a visiting professor at DISIM of University of LAquila in 2018. He has authored numerous articles on optimal process design and operation, AI-driven solutions for chemical process industries, and hydrogen-CO2-based economy.